Journal of Alloys and Compounds 513 (2012) 378–386

Contents lists available at SciVerse ScienceDirect

Journal of Alloys and Compounds

journal homepage: www.elsevier.com/locate/jallcom

The ternary Cr–Al–Nb phase diagram: Experimental investigations of isothermal sections at 1150, 1300 and 1450 °C

O. Prymak[1], F. Stein*

Max-Planck-Institut für Eisenforschung GmbH, D-40237 Düsseldorf, Germany

ARTICLE INFO

Article history:
Received 5 September 2011
Received in revised form 11 October 2011
Accepted 16 October 2011
Available online 25 October 2011

Keywords:
Intermetallics
Laves phases
Transition metal alloys and compounds
Phase diagrams
Phase transitions
Crystal structure

ABSTRACT

Isothermal sections of the ternary Cr–Al–Nb phase diagram were experimentally investigated for temperatures of 1150, 1300, and 1450 °C by electron-probe microanalysis (EPMA), X-ray diffraction (XRD), differential thermal analysis (DTA) and light-optical (LOM) as well as scanning electron microscopy (SEM). Cr–Al–Nb alloys were prepared by levitation melting and annealed at temperatures between 1150 and 1450 °C for up to 1500 h. The most striking feature of the ternary Cr–Al–Nb phase diagram is the extended phase field of the cubic *C*15 and the hexagonal *C*14 Laves phase $Nb(Cr,Al)_2$. With increasing Al content, the Laves phase polytype changes from *C*15 to *C*14. Both phase fields are separated by a small two-phase field, which shifts to lower Al contents with increasing temperature. The lattice parameters of both Laves phase polytypes and of all other phases occurring in this system were studied in dependence on composition and the solubilities of ternary elements in the binary phases were established.

1. Introduction

Transition-metal Laves phases are frequently discussed as attractive candidates for structural materials at very high temperatures, see e.g. [1–4]. Especially two-phase alloys on the basis of the Laves phase $NbCr_2$ have been studied because of the high melting point, relative low density, good high-temperature oxidation behaviour and very good high-temperature strength and creep resistance of $NbCr_2$ [5–10]. In order to improve the insufficient low-temperature deformability, the effect of the addition of ternary alloying elements has been investigated [11,12]. A candidate worth to be studied as alloying element is Al, because both the metal Cr as well as the Laves phase $NbCr_2$ can dissolve large amounts of Al [13,14]. As the knowledge of the phase equilibria in respective systems is an essential prerequisite for the development of materials on the basis of such alloys, the aim of the present work is an investigation of the high-temperature phase equilibria in the ternary Cr–Al–Nb system.

The phase diagrams of the three binary subsystems of the Cr–Al–Nb system are well described in the literature. The Cr–Nb binary system [15–20] consists of the two solid solutions (Cr) and (Nb) both forming a eutectic with the Laves phase $NbCr_2$, which is the only intermetallic phase of this system. Whereas the older literature reports on a phase transformation of the *C*15 Laves phase to the hexagonal *C*14 Laves phase polytype at about 1600 °C, the most recent investigations of the system indicate that the cubic *C*15 structure is stable up to the congruent melting point and the frequently observed hexagonal *C*14 polytype is a metastable phase [21]. The Al–Nb system [22–26] contains the congruently melting phase Al_3Nb and the two peritectically melting, Nb-rich phases $AlNb_2$ and $AlNb_3$. In the Al–Cr system [27–32], the (Cr) solid solution extends far into the binary system up to about 45 at.% Al at 1320 °C. Below 910 °C, the phase $AlCr_2$, which is the only Cr-rich intermetallic phase of the system, precipitates from the (Cr) solid solution. Above 50 at.% Al, a series of Al-rich intermetallic phases Al_8Cr_5, Al_9Cr_4, $Al_{11}Cr_4$, Al_4Cr, $Al_{11}Cr_2$, and Al_7Cr forms peritectically from the melt ($Al_{11}Cr_4$ forms peritectoidally). In this Al-rich part of the Al–Cr phase diagram, which is still not completely solved [30,31], all phases besides Al_8Cr_5 melt below 1100 °C. Therefore, they are not relevant for the present investigations, which focus on high-temperature phase equilibria above 1100 °C.

There are only few investigations on the ternary Cr–Al–Nb phase diagram available, which are summarized in [13,14]. Svechnikov et al. [33] studied the Nb-rich part of the ternary system in the composition triangle $Nb–NbCr_2–NbAl_3$ at 1200 and 1500 °C by metallography and X-ray diffraction (XRD) analysis of 46 ternary alloys. Analyses of the compositions of the observed phases were not performed. Besides this work of Svechnikov et al., there are only three more publications on experimental work, all of them

* Corresponding author. Tel.: +49 211 6792 557; fax: +49 211 6792 299.
E-mail address: stein@mpie.de (F. Stein).
[1] Present address: Institute for Inorganic Chemistry, University Duisburg-Essen, D-45117 Essen, Germany.

0925-8388/$ – see front matter © 2011 Elsevier B.V. All rights reserved.
doi:10.1016/j.jallcom.2011.10.053

Table 1
Nominal compositions of the investigated ternary Cr–Al–Nb alloys and phases identified by XRD in the as-cast condition and after heat treatments.

Alloy no.	Nominal composition			Phases identified by XRD			
	Cr (at.%)	Al (at.%)	Nb (at.%)	As-cast	1150 °C	1300 °C	1450 °C
1	70	5	25	*C*14 + (Cr)	*C*15 + (Cr)	*C*15 + (Cr)	*C*15 + (Cr)
2	60	9	31	*C*14 + (Cr)	*C*15 + (Cr)[a]	*C*15 + (Cr)[a]	*C*14 + (Cr)
3	56	24	20	*C*14 + (Cr)	*C*14 + (Cr)	*C*14 + (Cr)	*C*14 + (Cr)
4	31	48	21	*C*14 + Al_3Nb + $AlCr_2$	*C*14 + Al_3Nb + (Cr)	*C*14 + Al_3Nb + (Cr)	–[b]
5	52	3	45	*C*14 + (Nb)	*C*15 + (Nb)	–	–
6	40	5	55	*C*14 + (Nb)	*C*15 + (Nb) [a]	*C*15 + (Nb) [a]	*C*15 + (Nb) [a]
7	50	9	41	*C*14 + (Nb)	*C*15 + $AlNb_3$ [a]	*C*15 + $AlNb_3$ [a]	*C*14 + (Nb)
8	32	19	49	*C*14 + $AlNb_2$	*C*14 + $AlNb_2$	–	–
9	20	20	60	*C*14 + $AlNb_2$	*C*14 + $AlNb_2$ + $AlNb_3$	*C*14 + $AlNb_2$ + $AlNb_3$	*C*14 + $AlNb_2$ + Nb
10	20	32	48	*C*14 + $AlNb_2$	*C*14 + $AlNb_2$	*C*14 + $AlNb_2$	*C*14 + $AlNb_2$
11	10	50	40	*C*14 + $AlNb_2$ + Al_3Nb	*C*14 + $AlNb_2$ + Al_3Nb	*C*14 + $AlNb_2$ + Al_3Nb	*C*14 + $AlNb_2$ + Al_3Nb
12	56.7	10	33.3	*C*14	–	–	–
13	46.7	20	33.3	*C*14	–	–	–
14	36.7	30	33.3	*C*14	–	–	–

[a] Sample contains small amounts of metastable *C*14 phase; see text.
[b] Sample was partially molten.

dealing with the isothermal section at 1000 °C [34–36]. Hunt and Raman [34] only provided a rough overview of the system and the exact positions of the phase boundaries and the tie-triangles remained undefined as they only used XRD analysis. Mahdouk and Gachon [35] employed direct reaction calorimetry to prepare seven ternary samples from fine powders of the pure metals, which were annealed at 1000 °C for 168 h and then examined by XRD and electron probe microanalysis (EPMA). As the authors state themselves, the main drawback of their preparation method is the comparatively high level of impurities due to the use of fine powders. The third publication showing an isothermal section at 1000 °C is from Zhao et al. [36], who deduced their partial isothermal section from EPMA and electron backscatter diffraction (EBSD) results on a diffusion quadruple comprised of Cr, Nb, $NbAl_3$, and $NbSi_2$ which was heat treated at 1000 °C for 2000 h. The basic phase relationships in the three versions of the 1000 °C isothermal section are the same and consistent with the two isothermal sections at 1200 and 1500 °C reported by Svechnikov et al. [33]. The main discrepancies of the three isothermal sections at 1000 °C are the extensions of the various phase fields, especially the solubilities of Al in the *C*15 Laves phase, Nb in the ternary Laves phase, Cr and Al in the (Nb) solid solution, and Cr in Nb_3Al, Nb_2Al and $NbAl_3$.

The present investigation focuses on phase equilibria in the ternary Cr–Al–Nb system at 1150, 1300, and 1450 °C. Partial isothermal sections were already shown in a previous publication [37], where site occupations in the hexagonal *C*14 $Nb(Cr,Al)_2$ Laves phase were discussed. In parallel to the present experimental investigations, thermodynamic modelling applying the Calphad method has been performed on the basis of the available experimental data [38].

2. Experimental

Cr–Al–Nb alloys were prepared from high-purity metals (Nb 99.9 wt.%, Cr 99.99 wt.%, Al 99.999 wt.%) by crucible-free levitation melting in an argon atmosphere and drop-casting into cold copper moulds of 10 mm in diameter. The nominal compositions of the alloys are listed in Table 1. For heat treatments, cylindrical pieces of 10 mm in length were cut by electrical discharge machining (EDM), polished and cleaned in ethanol. For heat treatments at 1150 °C, samples were encapsulated in quartz ampoules, which were evacuated and back-filled with argon several times before sealing them. After the heat treatment at 1150 °C for 100 h (or, in some cases, 1500 h), the samples were quenched by breaking the ampoules in 10% NaCl brine. For heat treatments at 1300 °C (100 h) and 1450 °C (50 h), quartz ampoules cannot be used as they are no longer gas-tight. Instead, the samples were wrapped in Nb foil and placed into an alumina crucible with Ti filings as oxygen getter. The heat treatments were performed in an Ar atmosphere and finally the samples were rapidly cooled in a jet of Ar gas.

Chemical analysis of two selected samples (alloy 2, as-cast and after heat treatment at 1450 °C) gave carbon contents of 12 and 17 wt.ppm, oxygen contents of 22 and 150 wt.ppm, nitrogen contents of 8 and 38 wt.ppm, and silicon contents of 14 and 8 wt.ppm, respectively, showing that the impurity content of the as-cast alloys is low and does not change much during the heat treatments.

EPMA measurements were carried out with a Cameca SX 50 and a Jeol JXA-8100 instrument using pure Cr, Al, and Nb as standards. Phase compositions were analysed with a beam probing sample volumes of about 1 μm^3. The relative error of the resulting compositions is 1%. For each phase, 11–15 measurements were performed. The composition values and errors given in the tables throughout this paper are the average values and standard deviations. The actual bulk composition of the heat-treated alloys was determined by averaging the EPMA results of 900–1000 spot analyses per sample with spacings of 5 or 10 μm in three to four rectangular fields.

XRD investigations of crushed and powdered samples with particle sizes <90 μm were performed in Bragg-Brentano geometry using an "X'Pert" Philips PW-1827 diffractometer with CuK_α radiation ($\lambda = 0.154184$ nm) in a 2θ range from 10° to 110° with a step size of 0.02°. The lattice parameters were determined using the Rietveld refinement program package FullProf [39]. For the final accuracy of the lattice parameters, an error of ±0.0002 nm was estimated.

Differential thermal analysis (DTA) was carried out with a Setaram SETSYS-18 DTA (SETARAM, Caluire, France) allowing measurements up to 1750 °C. Cylindrical samples of 3 mm in diameter and height were placed in alumina crucibles and heated and cooled with rates of 5 and 10 K/min in an Ar atmosphere.

For metallographic observation of the microstructures, light-optical (LOM) and scanning electron microscopy (SEM) were used. For LOM investigations, the samples were etched with "Ti2", an etchant consisting of glycerine (68 vol.%), 70%–HNO_3 (16 vol.%), and 40%–HF (16 vol.%). SEM was performed using a Hitachi S-530 and a JEOL JSM 6500F electron microscope.

3. Results and discussion

The nominal compositions of the investigated alloys are listed in Table 1 together with all phases identified by XRD in the as-cast state and after heat treatments at 1150, 1300, and 1450 °C. Tables 2–4 give information about the analysed alloy compositions and the compositions and lattice parameters of each phase as determined by EPMA and XRD, respectively. The basic crystallographic information about the occurring phases as reported in [40] is summarized in Table 5. The resulting isothermal sections of the ternary Cr–Al–Nb phase diagram as established from the present experimental data for temperatures of 1150, 1300 and 1450 °C are shown in Figs. 1–3. The most striking feature of the phase diagram is the extended phase field of the Laves phase $Nb(Cr,Al)_2$, which cuts the isothermal sections more or less into two parts. Therefore, the following discussion is divided into three parts where the first one deals with the Nb-lean area covering the region between the Cr–Al boundary and the Laves phase, the second one focuses on the Laves phase, and the third part contains a discussion about the Nb-rich area of the phase diagram.

Table 2
Alloy and phase compositions as analysed by EPMA and lattice parameters determined by XRD after heat treatments at 1150 °C.

Alloy no.	Analysed alloy composition			Heat treatment time (h)	Phases	Phase composition			Lattice parameters	
	Cr (at.%)	Al (at.%)	Nb (at.%)			Cr (at.%)	Al (at.%)	Nb (at.%)	*a* (nm)	*c* (nm)
1	70.1	5.5	24.4	100	*C*15	61.7 ± 0.9	6.3 ± 0.8	32.0 ± 0.4	0.6992	
					(Cr)	93.1 ± 0.6	4.3 ± 0.4	2.6 ± 0.4	0.2892	
2	60.6	9.7	29.7	100	*C*15	56.1 ± 0.4	11.0 ± 0.6	32.9 ± 0.6	0.7016	
					(Cr)	[a]	[a]	[a]	0.2900	
					C14 [b]				0.4959	0.8123
2	60.6	9.7	29.7	1500	*C*15	58.1 ± 0.3	9.0 ± 0.2	32.9 ± 0.2	0.7013	
					(Cr)	92 ± 1	6.2 ± 0.2	2 ± 1	0.2898	
					C14[b]				0.4963	0.8090
3	54.3[c]	23.6[c]	22.1[c]	100	*C*14	42.2 ± 0.9	25.8 ± 0.6	32.0 ± 0.8	0.5010	0.8211
					(Cr)	80.2 ± 0.9	18.2 ± 0.4	1.6 ± 0.6	0.2938	
4	30.0	46.5	23.5	100	*C*14	26.3 ± 0.2	40.8 ± 0.2	32.9 ± 0.3	0.5055	0.8267
					Al_3Nb	1.6 ± 0.8	72.7 ± 0.6	25.7 ± 0.4	0.3838	0.8612
					(Cr)	65.5 ± 0.9	32.8 ± 0.5	1.7 ± 0.5	0.2973	
5	52[d]	3[d]	45[d]	1500	*C*15	61.4 ± 0.3	3.2 ± 0.1	35.4 ± 0.3	0.7011	
					(Nb)	11 ± 3	2.6 ± 0.1	87 ± 3	0.3273	
6	40.8	5.0	54.2	1500	*C*15	59.0 ± 0.4	5.5 ± 0.1	35.5 ± 0.4	0.7017	
					(Nb)	7.8 ± 0.5	4.1 ± 0.1	88.1 ± 0.5	0.3274	
					C14[b]				0.4961	0.8115
7	50.2	8.6	41.2	100	*C*15	57.0 ± 0.8	7.1 ± 0.2	35.8 ± 0.7	0.7028	
					$AlNb_3$	[a]	[a]	[a]	0.5178	
					C14[b]				0.4966	0.8132
7	50.2	8.6	41.2	1500	*C*15	58.0 ± 0.6	6.8 ± 0.2	35.2 ± 0.5	0.7024	
					$AlNb_3$	[a]	[a]	[a]	0.5176	
					C14[b]				0.4966	0.8120
8	31.3	21.1	47.5	1500	*C*14	50.2 ± 0.9	15.8 ± 0.6	34.0 ± 0.6	0.4978	0.8185
					$AlNb_2$	8.3 ± 0.7	28.4 ± 0.7	63.3 ± 0.6	0.9923	0.5138
9	22.0	20.3	57.7	1500	*C*14	53.7 ± 0.6	10.8 ± 0.5	35.5 ± 0.3	0.4978	0.8171
					$AlNb_2$	10.5 ± 0.8	23.6 ± 0.5	65.9 ± 0.8	0.9924	0.5138
					$AlNb_3$	[a]	[a]	[a]	0.5174	
10	19.7	31.0	49.3	100	*C*14	33.5 ± 0.6	31.3 ± 0.2	35.2 ± 0.7	0.5035	0.8245
					$AlNb_2$	5.4 ± 0.9	31.2 ± 0.1	63.4 ± 0.9	0.9925	0.5149
10	19.7	31.0	49.3	1500	*C*14	34.1 ± 0.5	30.9 ± 0.1	35.0 ± 0.5	0.5031	0.8245
					$AlNb_2$	7.9 ± 0.8	31.2 ± 0.1	60.9 ± 0.8	0.9921	0.5147
11	9.2	49.5	41.3	100	*C*14	20.3 ± 0.1	44.9 ± 0.2	34.8 ± 0.3	0.5076	0.8298
					$AlNb_2$	1.9 ± 0.3	35.8 ± 0.2	62.3 ± 0.9	0.9919	0.5164
					Al_3Nb	0.4 ± 0.1	73.3 ± 0.2	26.3 ± 0.2	0.3841	0.8614

[a] Particles too small for EPMA analyses.
[b] Sample contains small amounts of metastable *C*14 phase; see text.
[c] As analysed after 1300 °C heat treatment.
[d] Nominal composition.

3.1. The Nb-lean part of the ternary system

The solubility of Al in the (Cr) solid solution reaches very high values in the binary Cr–Al system and is above 40 at.% in the investigated temperature range (see, e.g. [31]). The ternary solubility of Nb in this solid solution remains small for all temperatures and Al contents. The maximum observed Nb content is 3.6 at.% at 1450 °C in an alloy with 22 at.% Al. The experimental data indicate a decrease of the Nb solubility both with decreasing temperature and Al content.

Between the (Cr) solid solution and the Laves phase $Nb(Cr,Al)_2$ there is an extended two-phase field characterizing the Cr-rich corner of the ternary phase diagram. The microstructure of heat-treated alloys in this composition range consists of a coarsened eutectic mixture of the two phases and a certain, composition-dependent amount of primary phase, which in case of the two representative examples shown in Fig. 4 is the Laves phase. DTA measurements and examinations of the as-cast microstructures indicate that there is a eutectic valley between the Laves phase and the (Cr) solid solution. Starting from the binary (Cr) + $NbCr_2$ eutectic at 18 at.% Nb and 1668 °C [16], the eutectic temperatures measured for the present alloys in this composition range continuously decrease with increasing Al content (alloy 1: 1633 °C, alloy 2: 1605 °C, alloy 3: 1534 °C).

At higher Al contents (Cr) solid solution and Laves phase form a three-phase field with the Al–Nb intermetallic phase Al_3Nb at 1150 and 1300 °C. The body-centred tetragonal $D0_{22}$-type Al_3Nb dissolves only small amounts of Cr (1150 °C: 1.6 at.%, 1300 °C: 1.3 at.%).

The Al corner of the ternary system was not investigated in detail as the liquid phase coming from the low-melting (Al) solid solution extends far into the ternary system at high temperatures. Alloy 4 (Cr–48 at.% Al–21 at.% Nb) is molten for the most part at 1450 °C. The boundaries of the liquid phase field in Figs. 1–3 are given as dotted lines as they are only tentative. The positions of the corners of the liquid phase field were estimated from the results of ongoing investigations of the liquidus surface of the system, which will be published elsewhere [41].

3.2. The ternary C15 and C14 Laves phase $Nb(Cr,Al)_2$

The solubility of Al in the cubic *C*15 Laves phase $NbCr_2$ amounts to about 11 at.% Al at 1150 °C and decreases with increasing temperature. At higher Al contents, the hexagonal *C*14 Laves phase polytype occurs and forms a phase field which extends far into the ternary system parallel to the Cr–Al axis (Figs. 1–3), i.e., Al preferentially replaces Cr. Such a change of the stable Laves phase polytype from *C*15 to *C*14 in case of a partial substitution of the B atoms of a Laves phase AB_2 by a ternary element C is a frequently observed feature of ternary Laves phase-containing phase diagrams (see [42]) and is related to the higher flexibility of the *C*14 crystal structure to accommodate ternary elements as has been discussed in Ref. [43].

Table 3
Alloy and phase compositions as analysed by EPMA and lattice parameters determined by XRD after heat treatments at 1300 °C.

Alloy no.	Analysed alloy composition			Heat treatment time (h)	Phases	Phase composition			Lattice parameters	
	Cr (at.%)	Al (at.%)	Nb (at.%)			Cr (at.%)	Al (at.%)	Nb (at.%)	*a* (nm)	*c* (nm)
1	70.1[a]	5.5[a]	24.4[a]	100	*C*15	62.5 ± 0.3	5.3 ± 0.1	32.2 ± 0.4	0.6995	
					(Cr)	94.6 ± 0.2	4.0 ± 0.1	1.4 ± 0.2	0.2897	
2	60.4	9.7	29.9	100	*C*15	58.3 ± 0.5	9.1 ± 0.5	32.6 ± 0.2	0.7012	
					(Cr)	91.3 ± 0.3	7.1 ± 0.2	1.6 ± 0.2	0.2903	
					C14[c]				0.4952	0.8139
3	54.3	23.6	22.1	100	*C*14	43.0 ± 0.6	24.7 ± 0.6	32.3 ± 0.2	0.5000	0.8211
					(Cr)	78.1 ± 0.6	19.9 ± 0.6	2.0 ± 0.2	0.2944	
4	30.0[a]	46.5[a]	23.5[a]	100	*C*14	26.6 ± 0.2	40.9 ± 0.1	32.5 ± 0.2	0.5050	0.8273
					Al_3Nb	1.3 ± 0.1	72.7 ± 0.2	26.0 ± 0.2	0.3836	0.8621
					(Cr)	65.6 ± 0.5	32.8 ± 0.4	1.6 ± 0.2	0.2974	
6	40.8[a]	5.0[a]	54.2[a]	100	*C*15	58.6 ± 0.4	5.4 ± 0.1	36.0 ± 0.4	0.7023	
					(Nb)	11 ± 1	4.4 ± 0.1	85 ± 1	0.3268	
					C14[c]				0.4966	0.8124
7	50.2[a]	8.6[a]	41.2[a]	100	*C*15	56.9 ± 0.2	7.8 ± 0.1	35.3 ± 0.1	0.7035	
					$AlNb_3$	[b]	[b]	[b]	0.5170	
					C14[c]				0.4971	0.8150
9	26.9	18.6	54.5	100	*C*14	50 ± 1	13.8 ± 0.9	35.9 ± 0.5	0.4976	0.8196
					$AlNb_2$	11 ± 1	23.0 ± 0.9	66 ± 1	0.9910	0.5135
					$AlNb_3$	[b]	[b]	[b]	0.5168	
10	19.7[a]	31.0[a]	49.3[a]	100	*C*14	33.7 ± 0.2	31.3 ± 0.1	35.0 ± 0.2	0.5030	0.8263
					$AlNb_2$	5.3 ± 0.3	30.9 ± 0.1	63.8 ± 0.3	0.9913	0.5138
11	9.2[a]	49.5[a]	41.3[a]	100	*C*14	19.8 ± 0.3	45.4 ± 0.4	34.8 ± 0.4	0.5071	0.8317
					$AlNb_2$	2.4 ± 0.3	37.1 ± 0.2	60.5 ± 0.4	0.9904	0.5166
					Al_3Nb	0.5 ± 0.1	73.2 ± 0.2	26.3 ± 0.3	0.3841	0.8617

[a] As analysed after 1150 °C heat treatment.
[b] Particles too small for EPMA analyses.
[c] Sample contains small amounts of metastable *C*14 phase; see text.

Table 4
Alloy and phase compositions as analysed by EPMA and lattice parameters determined by XRD after heat treatments at 1450 °C.

Alloy no.	Analysed alloy composition			Heat treatment time (h)	Phases	Phase composition			Lattice parameters	
	Cr (at.%)	Al (at.%)	Nb (at.%)			Cr (at.%)	Al (at.%)	Nb (at.%)	*a* (nm)	*c* (nm)
1	70.1[a]	5.5[a]	24.4[a]	50	*C*15	63.2 ± 0.2	4.9 ± 0.3	31.9 ± 0.2	0.6993	
					(Cr)	93.4 ± 0.4	4.3 ± 0.3	2.3 ± 0.2	0.2902	
2	60.6[a]	9.7[a]	29.7[a]	50	*C*14	59.6 ± 0.3	8.6 ± 0.1	31.8 ± 0.3	0.4942	0.8136
					(Cr)	89.9 ± 0.7	7.2 ± 0.1	2.9 ± 0.8	0.2907	
3	54.3[a]	23.6[a]	22.1[a]	50	*C*14	44.6 ± 0.1	24.1 ± 0.2	31.3 ± 0.2	0.4991	0.8197
					(Cr)	74.4 ± 0.5	22.0 ± 0.2	3.6 ± 0.4	0.2953	
4	30.0[a]	46.5[a]	23.5[a]	50	[b]					
6	40.8[a]	5.0[a]	54.2[a]	50	*C*15	58.6 ± 0.1	5.2 ± 0.1	36.2 ± 0.1	0.7033	
					(Nb)	14 ± 1	4.8 ± 0.1	80.8 ± 0.4	0.3253	
					C14[c]				0.4971	0.8140
7	50.2[a]	8.6[a]	41.2[a]	50	*C*14	54.6 ± 0.2	8.9 ± 0.1	36.5 ± 0.2	0.4968	0.8200
					(Nb)	13.8 ± 0.3	7.5 ± 0.1	78.7 ± 0.3	0.3252	
9	18.9	19.6	61.5	50	*C*14	50.8 ± 0.7	12.8 ± 0.8	36.4 ± 0.2	0.4978	0.8207
					$AlNb_2$	13.9 ± 0.7	20.4 ± 0.7	65.7 ± 0.7	0.9885	0.5124
					(Nb)	13.5 ± 0.1	10.0 ± 0.5	76.5 ± 0.4	0.3265	
10	19.7[a]	31.0[a]	49.3[a]	50	*C*14	33.5 ± 0.3	31.4 ± 0.2	35.1 ± 0.3	0.5031	0.8267
					$AlNb_2$	7.6 ± 0.1	30.5 ± 0.1	61.9 ± 0.2	0.9892	0.5122
11	9.2[a]	49.5[a]	41.3[a]	50	*C*14	19.6 ± 0.3	45.6 ± 0.3	34.8 ± 0.4	0.5072	0.8324
					$AlNb_2$	3.7 ± 0.1	40.5 ± 0.2	55.8 ± 0.4	0.9868	0.5165
					Al_3Nb	0.6 ± 0.1	72.9 ± 0.2	26.4 ± 0.1	0.3841	0.8615

[a] As analysed after 1150 °C heat treatment.
[b] Sample was partially molten.
[c] Sample contains small amounts of metastable *C*14 phase; see text.

Table 5
Crystallographic data of all phases occurring in the investigated temperature range [40]. The composition dependence of the lattice parameters of the ternary *C*14 Laves phase is discussed in Section 3.2.

Phase	Structure type	Pearson symbol	Space group	Strukturbericht designation	Lattice parameters [nm]
(Cr)	W	*cI*2	$Im\bar{3}m$	*A*2	$a = 0.2884$
(Nb)	W	*cI*2	$Im\bar{3}m$	*A*2	$a = 0.3300$
β-Al_8Cr_5	Cu_5Zn_8	*cI*52	$I\bar{4}3m$	$D8_2$	$a = 0.9065$
Al_3Nb	Al_3Ti	*tI*18	*I*4/*mmm*	$D0_{22}$	$a = 0.3844$ $c = 0.8605$
$AlNb_2$	σCrFe	*tP*30	$P4_2/mnm$	$D8_b$	$a = 0.9943$ $c = 0.5186$
$AlNb_3$	Cr_3Si	*cP*8	$Pm\bar{3}n$	*A*15	$a = 0.5186$
$NbCr_2$ (*C*15)	$MgCu_2$	*cF*24	$Fd\bar{3}m$	*C*15	$a = 0.6991$
$Nb(Cr,Al)_2$ (*C*14)	$MgZn_2$	*hP*12	$P6_3/mmc$	*C*14	

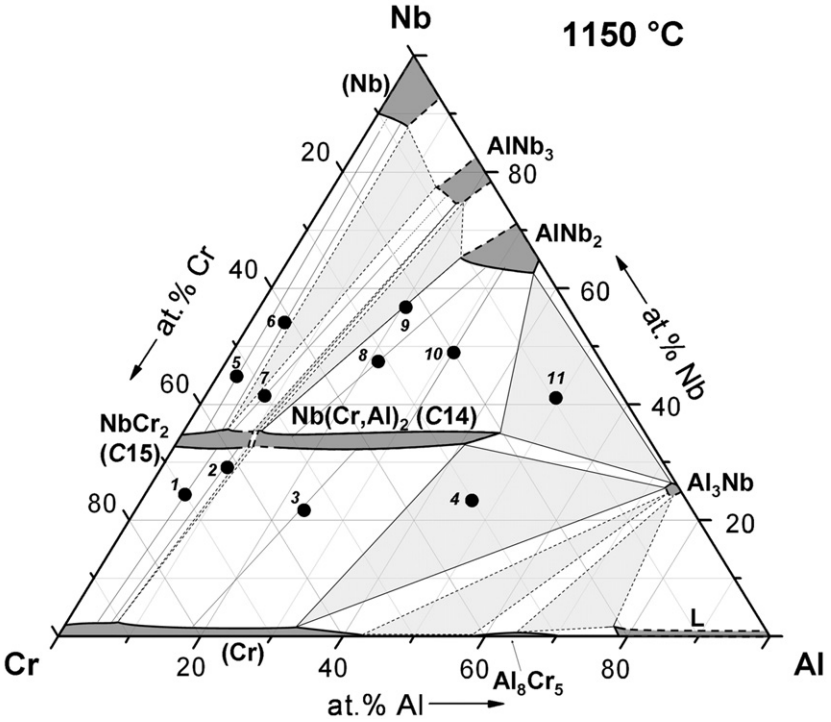

Fig. 1. Isothermal section of the Cr–Al–Nb system at 1150 °C. The black circles mark the compositions of the investigated alloys.

The solubility of Al in the *C*14 Laves phase is at about 45 at.% Al for all investigated temperatures. The same value was also reported by Zhao et al. [36] for a temperature of 1000 °C. A similar temperature-independence of the Al solubility was also found in the ternary Laves phases $Nb(Co,Al)_2$ [44] and $Nb(Fe,Al)_2$ [45].

According to Thoma and Perepezko [16], the width of the homogeneity range of the binary *C*15 Laves phase is 1.8 at.% at 1100 °C (32.5–34.3 at.% Nb) and 4.4 at.% at 1400 °C (32.0–36.4 at.% Nb). The present results show that this width remains nearly unchanged on alloying with Al. For both the *C*15 and the *C*14 phase, the average width of the homogeneity range is about 2 at.% Nb at 1150 °C and 4.5 at.% Nb at 1450 °C.

The extension of the small two-phase region between the *C*15 and *C*14 Laves phase is difficult to determine experimentally. From the present results, we can suppose the width of the two-phase region to be below 2 at.%. Due to the shift of the two-phase field

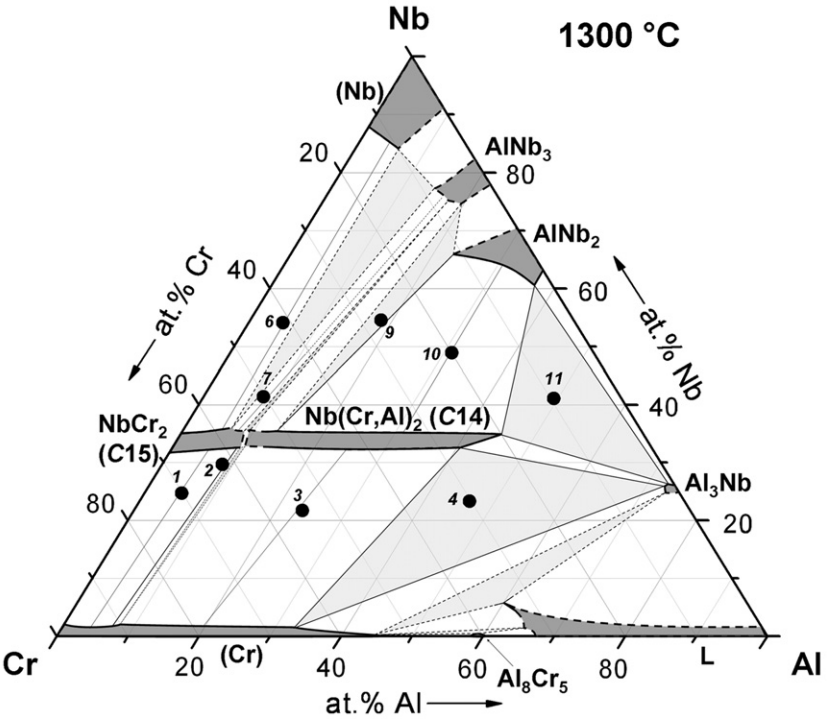

Fig. 2. Isothermal section of the Cr–Al–Nb system at 1300 °C. The black circles mark the compositions of the investigated alloys.

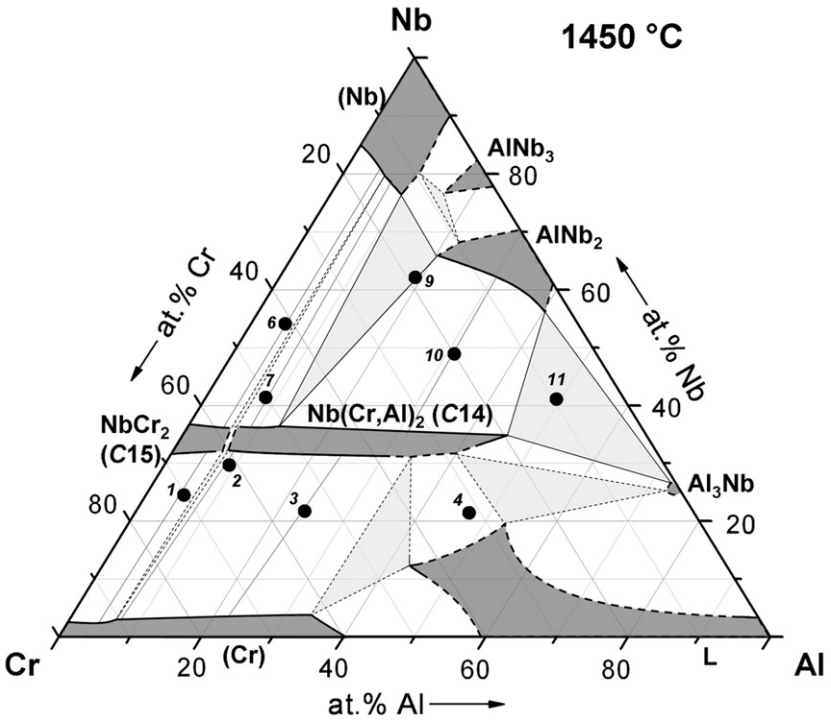

Fig. 3. Isothermal section of the Cr–Al–Nb system at 1450 °C. The black circles mark the compositions of the investigated alloys.

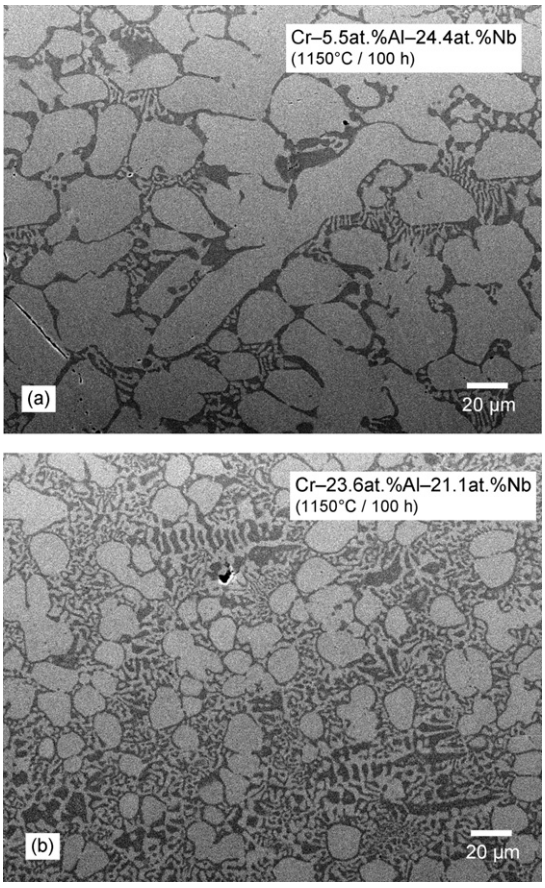

Fig. 4. SEM back-scattered electron micrographs of the microstructures of (a) alloy 1 (Cr–5.5 at.% Al–24.4 at.% Nb) and (b) alloy 3 (Cr–23.6 at.% Al–21.1 at.% Nb) after heat treatment at 1150 °C for 100 h and water quenching showing primary *C*15 (alloy 1) or *C*14 (alloy 3) Laves phase surrounded by coarsened (Cr) + Laves phase eutectic.

to lower Al contents with increasing temperatures, alloys in this composition range show a transformation of the stable Laves phase polytype from *C*15 to *C*14 on heating. Fig. 5 shows XRD patterns of alloy 2 clearly revealing that the stable Laves phase polytype is *C*15 at 1150 and 1300 °C (with some remnants of metastable *C*14, see last two paragraphs of this section) and completely transforms to *C*14 at 1450 °C.

On replacing Cr atoms by the larger Al atoms, the lattice parameters *a* and *c* of the stable *C*14 Laves phase increase nearly linearly as a function of the Al content (Fig. 6a). Rietveld refinements have shown that this replacement of Cr atoms by Al atoms happens preferentially on the 2*a* sites of the *C*14 lattice, which are completely occupied by Cr atoms in the binary case [37]. From crystallographic considerations it has been concluded in [43] that in case of such a 2*a* site preference of the larger Al atoms, the *c*/*a* ratio should decrease with increasing Al content as is confirmed in Fig. 6b. In order to compare the crystallographic parameters of the cubic *C*15 and hexagonal *C*14 Laves phases, the volumes per atom were plotted in Fig. 6c as a function of the Al content. For the *C*15 binary Laves phase, a lattice parameter of $a = 0.6991$ nm was taken from the literature [46]. The data indicate that the volumes per atom increase approximately linearly and independently of the structure type, i.e., the change of the stable structure type from cubic *C*15 to hexagonal *C*14 has no effect on the continuous increase. This behaviour can be explained by the strong similarity of the *C*14 and *C*15 crystal lattices and was also observed in other Laves phase systems as Co–Al–Nb [44] or Fe–Al–Zr [47].

In all as-cast alloys the *C*14 Laves phase polytype is present. In case of the Al-poor alloys with less than about 10 at.% Al, the *C*14 phase is only metastable and probably is a result of the casting process. As described above, the amount of Al needed to stabilize the *C*14 Laves phase decreases with increasing temperature, i.e., the C14 phase field grows more and more in the direction of the binary Cr–Nb boundary on raising the temperature. Therefore, during casting of Al-poor alloys at first *C*14 Laves phase precipitates from the melt and then transforms to *C*15 Laves phase at lower temperature in the equilibrium case. Fig. 7 shows some large,

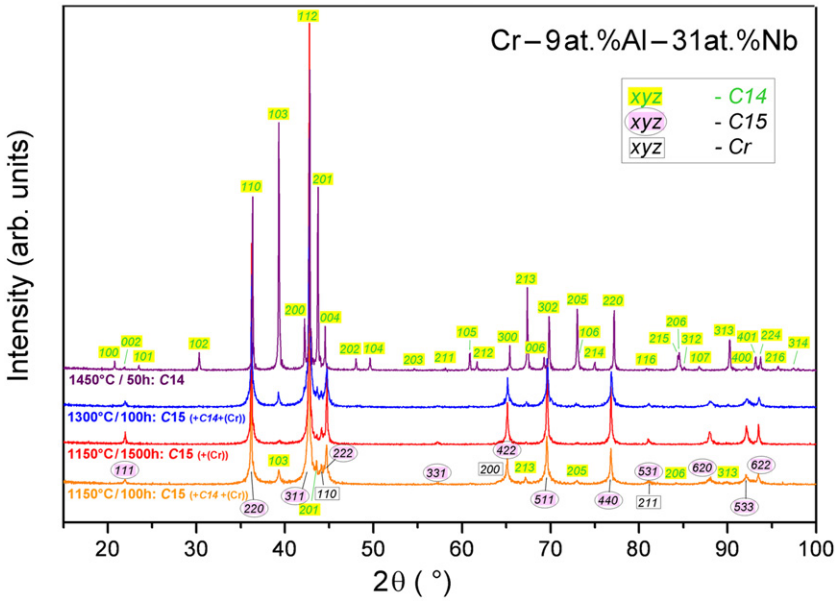

Fig. 5. X-ray analysis of alloy 2 (nominal composition Cr–9 at.% Al–31 at.% Nb) showing the transition from the *C*15 to the *C*14 Laves phase polytype with increasing temperature of the heat treatment (upper three plots) as well as the disappearance of the metastable *C*14 phase at 1150 °C after long-term heat treatment (lower two plots).

heavily twinned *C*15 grains in the nearly single-phase Laves phase alloy 2 after 100 h heat treatment at 1150 °C. According to [48,49], this twinning is a consequence and clear indication of the *C*14-to-*C*15 transformation. Due to the fact that the diffusion-controlled, solid-state *C*14 → *C*15 transformation is very slow, *C*14 is retained at room temperature and dissolves only slowly during the heat treatments. Fig. 5 shows a comparison of XRD patterns obtained from alloy 2 after heat treatments at 1150 °C for 100 and 1500 h. Whereas after 100 h the additional lines of the hexagonal *C*14 phase are still clearly visible besides the strong *C*15 peaks, no or only very weak characteristic lines of the *C*14 phase can be detected after 1500 h.

As was already mentioned in [37], another clear indication of the metastability of the Al-poor *C*14 phase is the fact that the *c*/*a* ratios strongly deviate from the continuous behaviour of the equilibrium *C*14 phase shown in Fig. 6b. For example, the *c*/*a* ratio of the metastable *C*14 phase in alloy 7 (approximately 7 at.% Al) is 1.638 after 100 h, which is significantly below the value that could be expected from Fig. 6b, and reduces further to 1.635 after 1000 h heat treatment. Simple geometrical considerations on the packing of hard spheres show that the ideal *c*/*a* ratio which is needed for a close packing of hard spheres in a *C*14 structure is 1.633 (=$\sqrt{(8/3)}$) which corresponds to the theoretical value of a *C*15 structure in hexagonal setting (see, e.g. [50]). Therefore, the observed decrease of the *c*/*a* ratio can be understood as an indication that the metastable *C*14 Laves phase is on the way to transform to the *C*15 equilibrium state.

3.3. The Nb-rich part of the ternary system

At 1450 °C, the (Nb) solid solution and $AlNb_2$ form a two-phase field. Therefore, the Nb-rich phase $AlNb_3$ can only co-exist with (Nb) and/or $AlNb_2$ but cannot be in equilibrium with the Laves phase. However, at 1150 and 1300 °C the cubic *A*15-type phase $AlNb_3$ was clearly identified by XRD in several heat-treated alloys forming a two-phase field with the *C*15 Laves phase, see Figs. 1–3. This finding of equilibria between $AlNb_3$ and the Laves phase at the lower heat treatment temperatures is different from the results reported in [33] for 1200 °C and in [35,36] for 1000 °C, where the Laves phase is found to be only in equilibrium with (Nb) and $AlNb_2$ but not with $AlNb_3$. If the present results are correct, a reaction of the type *C*15 + $AlNb_3$ ↔ *C*14 + (Nb) must take place at a certain temperature between 1300 and 1450 °C. Indeed, DTA measurements of alloy 7, which had been heat-treated at 1150 °C prior to the experiment in order to obtain a two-phase *C*15 + $AlNb_3$ starting microstructure, show a clearly visible peak with an onset at 1389 °C, which can be attributed to the transformation to *C*14 + (Nb) (Fig. 8). A DTA experiment with the same alloy in the as-cast state, which neither contains *C*15 Laves phase nor $AlNb_3$ but is *C*14 + (Nb) (Table 1), shows no such effect. This is another hint indicating that the DTA effect at 1389 °C is related to the above reaction. In addition, Fig. 8 shows the measured tie lines of the heat-treated alloy, which are more or less parallel at 1150 and 1300 °C, whereas the tie line at 1450 °C clearly shows a different orientation connecting the *C*14 Laves phase with the (Nb) solid solution.

Obviously $AlNb_3$ is a very slowly forming phase, it never occurs in the as-cast state and even after the longest heat treatment times forms only small grains (<1 μm), which are too fine to be analysed by EPMA. For that reason, an exact value for the solubility of Cr in this phase cannot be given. The atomic radius of Cr is smaller than those of Al and Nb. Therefore, it can be expected that the addition of Cr to $AlNb_3$ and $AlNb_2$ results in a decrease of the lattice parameters what is confirmed by comparing the present results for the ternary alloys (Tables 2–4) with literature data for the binary phases (Table 5). Assuming that the effect of Cr on the shrinkage of the lattice is similar for $AlNb_3$ and $AlNb_2$, the measured lattice parameters indicate that the Cr solubility in $AlNb_3$ must be lower than in $AlNb_2$.

In case of the $AlNb_2$ phase, the solubility for Cr amounts to about 8 at.% at 1150 °C and increases with temperature to about 14 at.% at 1450 °C.

4. Summary

Isothermal sections of the ternary Cr–Al–Nb phase diagram were established for temperatures of 1150, 1300 and 1450 °C and the lattice parameters of all phases have been determined in dependence on composition.

The main characteristic of the ternary phase diagram is the extended phase field of the $Nb(Cr,Al)_2$ Laves phase. The hexagonal *C*14 Laves phase is the only ternary intermetallic phase of the

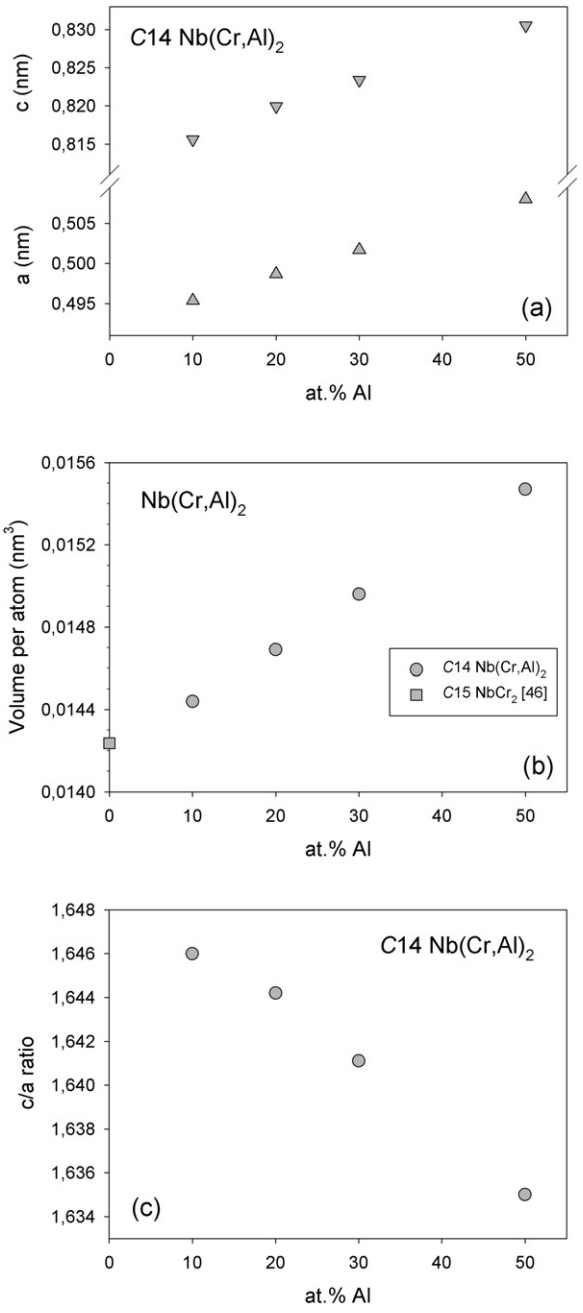

Fig. 6. Room-temperature lattice parameters a and c, volume per atom, and c/a ratio of as-cast, stoichiometric $Nb(Cr,Al)_2$ Laves phase as a function of the Al content. The volume per atom of $C15$ $NbCr_2$ was calculated from the literature value $a = 0.6991$ nm [46].

system and can dissolve up to 45 at.% Al at all investigated temperatures. The solubility of Al in the $C15$ Laves phase only amounts to about 11 at.% at 1150 °C and decreases to about 7 at.% at 1450 °C. With respect to the Nb content, the homogeneity range of the Laves phases broadens with increasing temperature but is nearly independent of the Al content. The volumes per atom of the $C15$ and $C14$ Laves phase increase nearly linearly with increasing Al content, and this increase is not affected by the change of the stable structure type from $C15$ to $C14$. The c/a ratio of the $C14$ Laves phase is larger than the ideal value of 1.633 and decreases with increasing Al content.

Whereas earlier versions of the Nb-rich part of the phase diagram show a three phase region $AlNb_2$–$AlNb_3$–Nb at 1200 °C [33]

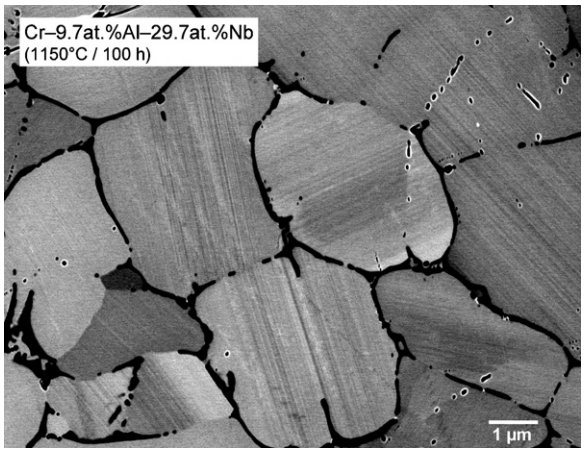

Fig. 7. SEM back-scattered electron micrograph of $C15$ Laves phase grains in alloy 2 (Cr–9.7 at.% Al–29.7 at.% Nb) after heat treatment at 1150 °C. The heavily twinned microstructure is a result of the metastable-$C14$ to stable-$C15$ transformation.

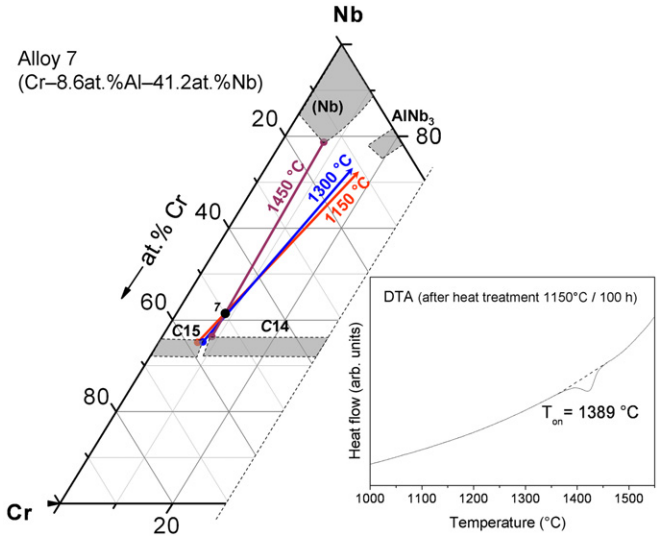

Fig. 8. Detail of the DTA heating curve of alloy 7 (Cr–8.6 at.% Al–41.2 at.% Nb) heat-treated at 1150 °C and tie lines of this alloy at 1150, 1300 and 1450 °C as measured by EPMA.

and 1000 °C [35,36], the present results reveal that this three-phase field only exists at the highest investigated temperature of 1450 °C and the solid state reaction $C15 + AlNb_3 \leftrightarrow C14 + (Nb)$ leads to the occurrence of the two-phase equilibrium $C15 + AlNb_3$ at 1300 and 1150 °C making the co-existence of (Nb) and $AlNb_2$ impossible.

Acknowledgments

This work was supported by the Max Planck Society within the framework of the inter-institutional research initiative “The Nature of Laves Phases”. The authors are grateful to Mr. Michael Kulse for synthesis of the alloys, Mrs. Heidi Bögershausen for preparation of metallographic sections, Dr. Stefan Zaefferer for taking one of the SEM micrographs and Mrs. Irina Wossack for EPMA analyses.

References

[1] J.D. Livingston, Phys. Status Solidi (a) 131 (1992) 415–423.
[2] G. Sauthoff, Intermetallics, VCH, Weinheim, Germany, 1995, 1–165.
[3] C.T. Liu, J.H. Zhu, M.P. Brady, C.G. McKamey, L.M. Pike, Intermetallics 8 (2000) 1119–1129.
[4] K.S. Kumar, Mater. Res. Soc. Symp. Proc. 460 (1997) 677–688.
[5] M. Takeyama, C.T. Liu, Mater. Sci. Eng. A 132 (1991) 61–66.

[6] D.M. Shah, D.L. Anton, D.P. Pope, S. Chin, Mater. Sci. Eng. A 192–193 (1995) 658–672.
[7] T. Takasugi, K.S. Kumar, C.T. Liu, E.H. Lee, Mater. Sci. Eng. A 260 (1999) 108–123.
[8] Y. Ohta, Y. Nakagawa, Y. Kaneno, H. Inoue, T. Takasugi, J. Mater. Sci. 38 (2003) 657–665.
[9] H. Zheng, S. Lu, Q. Su, F. Quan, Int. J. Refract. Met. Hard Mater. 26 (2008) 1–4.
[10] X. Xiao, S.Q. Lu, P. Hu, M.G. Huang, X.W. Nie, M.W. FU, Mater. Sci. Eng. A 485 (2008) 80–85.
[11] C.T. Liu, P.F. Tortorelli, J.A. Horton, C.A. Carmichael, Mater. Sci. Eng. A 214 (1996) 23–32.
[12] T. Takasugi, M. Yoshida, S. Hanada, Acta Mater. 44 (1996) 669–674.
[13] V. Ivanchenko, in: G. Effenberg, S. Ilyenko (Eds.), Landolt-Börnstein, New Series IV/11A1, SpringerMaterials, 2004, pp. 360–370, doi:10.1007/10915943_32, The Landolt-Börnstein Database, www.springermaterials.com.
[14] V. Raghavan, J. Phase Equilib. Diffus. 29 (2008) 173–174.
[15] M. Venkatraman, J.P. Neumann, in: T.B. Massalski, H. Okamoto, P.R. Subramanian, L. Kacprzak (Eds.), Binary Alloy Phase Diagrams, 2nd ed., ASM, Materials Park, OH, 1990, pp. 1298–1299.
[16] D.J. Thoma, J.H. Perepezko, Mater. Sci. Eng. A 156 (1992) 97–108.
[17] J.G. Costa Neto, S.G. Fries, H.L. Lukas, S. Gama, G. Effenberg, Calphad 17 (1993) 219–228.
[18] H. Okamoto, J. Phase Equilib. 14 (1993) 534–535.
[19] P. Franke, D. Neuschütz, in: P. Franke, D. Neuschütz (Eds.), Landolt-Börnstein, New Series IV/19B2, SpringerMaterials, 2004, pp. 1–3, doi:10.1007/10757405_85, The Landolt-Börnstein Database, www.springermaterials.com.
[20] J. Pavlu, J. Vrestal, M. Sob, Calphad 33 (2008) 179–186.
[21] J. Aufrecht, A. Leineweber, A. Senyshyn, E.J. Mittemeijer, Scr. Mater. 62 (2010) 227–230.
[22] J.L. Jorda, R. Flükiger, J. Muller, J. Less Common Met. 75 (1980) 227–239.
[23] U.R. Kattner, in: T.B. Massalski, H. Okamoto, P.R. Subramanian, L. Kacprzak (Eds.), Binary Alloy Phase Diagrams, 2nd ed., ASM, Materials Park, OH, 1990, pp. 179–181.
[24] C. Servant, I. Ansara, J. Chim. Phys. 94 (1997) 869–888.
[25] Z. Zhu, Y. Du, L. Zhang, H. Chen, H. Xu, C. Tang, J. Alloys Compd. 460 (2008) 632–638.
[26] V.T. Witusiewicz, A.A. Bondar, U. Hecht, T.Y. Velikanova, J. Alloys Compd. 472 (2009) 133–161.
[27] J. Murray, J. Phase Equilib. Diffus. 19 (1998) 368–375.
[28] K. Mahdouk, J.C. Gachon, J. Phase Equilib. Diffus. 21 (2000) 157–166.
[29] B. Grushko, E. Kowalska-Strzeciwilk, B. Przepiórzynski, M. Surowiec, J. Alloys Compd. 402 (2005) 98–104.
[30] B. Grushko, B. Przepiórzynski, D. Pavlyuchkov, J. Alloys Compd. 454 (2008) 214–220.
[31] H. Okamoto, J. Phase Equilib. Diffus. 29 (2008) 112–113.
[32] Y. Liang, C. Guo, C. Li, Z. Du, J. Alloys Compd. 460 (2008) 314–319.
[33] V.N. Svechnikov, A.K. Shurin, G.P. Dimitrieva, Issledovaniya Stali i Splavov (Investigation of Steels and Alloys), Publ. Nauka, Moscow, 1964, pp. 104–107.
[34] C.R. Hunt, A. Raman, Z. Metallkd. 59 (1968) 701–707.
[35] K. Mahdouk, J.C. Gachon, J. Alloys Compd. 321 (2001) 232–236.
[36] J.-C. Zhao, M.R. Jackson, L.A. Peluso, J. Phase Equilib. 25 (2004) 152–159.
[37] O. Prymak, F. Stein, A. Kerkau, A. Ormeci, G. Kreiner, G. Frommeyer, D. Raabe, Mater. Res. Soc. Symp. Proc. 1128 (2009) 499–504.
[38] C. He, F. Stein, Int. J. Mater. Res. 101 (2010) 1369–1375.
[39] J. Rodriguez-Carvajal, FullProf: A Program for Rietveld Refinement and Profile Matching Analysis of Complex Powder Diffraction Patterns, 2010, http://www.ill. eu/sites/fullprof/.
[40] P. Villars, L.D. Calvert, Pearson's Handbook of Crystallographic Data for Intermetallic Phases, 2nd ed., ASM International, Materials Park, OH, USA, 1991.
[41] F. Stein, C. He, unpublished results, 2011.
[42] F. Stein, M. Palm, G. Sauthoff, Intermetallics 13 (2005) 1056–1074.
[43] F. Stein, Mater. Res. Soc. Symp. Proc. 1295 (2011) 299–310.
[44] O. Dovbenko, F. Stein, M. Palm, O. Prymak, Intermetallics 18 (2010) 2191–2207.
[45] O. Prymak, F. Stein, unpublished results (2011).
[46] Z. Blažina, R. Trojko, J. Less Common Met. 119 (1986) 297–305.
[47] F. Stein, G. Sauthoff, M. Palm, Z. Metallkd. 95 (2004) 469–485.
[48] B.P. Bewlay, J.A. Sutliff, M.R. Jackson, H.A. Lipsitt, Acta Metall. Mater. 42 (1994) 2869–2878.
[49] K.S. Kumar, P.M. Hazzledine, Intermetallics 12 (2004) 763–770.
[50] D.J. Thoma, in: K.H.J. Buschow, R.W. Cahn, M.C. Flemmings, B. Ilschner, E.J. Kramer, S. Mahajan (Eds.), Encyclopedia of Materials: Science and Technology, Elsevier, Amsterdam, 2001, pp. 4205–4213.